Journal of Membrane Science 693 (2024) 122347

Contents lists available at ScienceDirect

Journal of Membrane Science

journal homepage: www.elsevier.com/locate/memsci

Ion-pairing design of covalent organic framework membranes for separation and controlled release of pharmaceuticals

Xingyuan Wang [a], Xiansong Shi [a,**], Zhe Zhang [a], Congcong Yin [a,b], Zhipeng Zhang [a], Yong Wang [a,b,*]

[a] State Key Laboratory of Materials-Oriented Chemical Engineering, College of Chemical Engineering, Nanjing Tech University, Nanjing, 211816, Jiangsu, PR China
[b] School of Energy and Environment, Southeast University, Nanjing, 210096, Jiangsu, PR China

ARTICLE INFO

Keywords:
Ion-pairing
Covalent organic frameworks
Host-guest interaction
Pharmaceutical
Nanopores

ABSTRACT

Intrinsically charged covalent organic frameworks (COFs) afford specific ionic nanochannels for mass transport, and thus become promising platforms to design membranes with unique selectivity. However, internal electrostatic repulsion and large-pore frameworks cause significant barriers that greatly limit membrane performances. Herein, we report a novel strategy to synchronously crystallize and upgrade cationic COF membranes by ion-pairing design. Ion-paired guest molecules are involved in electric-driven interfacial crystallization to offset the charges of the ionic monomers and host frameworks. This host-guest neutralization promotes the crystallization of compact COF membranes. Lateral dimension and charge nature of guest molecules fundamentally affect the ion-pairing efficiency. Tight encapsulation of the large-sized electronegative molecules effectually narrows the molecular sieving channels, yielding a significant elevation in membrane selectivity. The membrane rejection of organic ions with a size larger than 1.2 nm thus can be improved from below 50 % to above 85 % with a water permeance of ~10 L m^{-2} h^{-1} bar^{-1}. Prominently, our membranes demonstrate efficient recovery and pH-dependent release of bioactive pharmaceuticals, with a release rate that is 12 times higher in an acidic solution compared to a neutral environment. This work provides an ion-pairing strategy to regulate COF membranes for pharmaceutical industries and beyond.

1. Introduction

The growing demand of selective molecular and ionic separations in liquids has stimulated the fundamental and practical research of nanofiltration (NF) membranes in widespread areas [1]. In the past decade, significant efforts have been devoted to improving the overall performance of NF membranes to meet the increasingly challenging separation tasks. The development of molecularly thin membranes represents a breakthrough in NF techniques and inspires numerous follow-up studies [2,3]. On-demand NF processes are now available by processing smart materials into continuous and robust membranes [4–7]. Moreover, post-synthetic modification is also developed to finely tune the pore chemistry and configuration of NF membranes [8,9]. As a great advance in this field, porous materials featuring regular structures have been explored to innovate NF technologies [10–13]. Inspired by these structure-specific materials, particular attempts have been made to regulate the interfacial polymerization of traditional polymers to homogenize the originally irregular pores [14,15]. These previous reports highlight that the exploration of structure-uniform materials is of great significance for advancing NF membranes.

Covalent organic frameworks (COFs) are representative porous crystalline materials built from linking organic monomers through reticular chemistry [16,17]. Taking advantages of their regular and tailorable pores, COFs offer special potential to produce new-generation NF membranes for selective separation of molecules and ions [18–20]. For instance, their highly ordered pores with designable aperture sizes in the range of approximately 1–5 nm can perform accurate sieving of complex mixtures with minimal differences in dimensions [21]. The excellent resistance to solvents further promises their viable application for NF-based molecular separation in organic liquids [22]. Typically, the structure and functionality of monomers determine the characteristic of the resulting frameworks and thus the potency of COF-based NF

* Corresponding author. State Key Laboratory of Materials-Oriented Chemical Engineering, College of Chemical Engineering, Nanjing Tech University, Nanjing, 211816, Jiangsu, PR China.
** Corresponding author.
E-mail addresses: xsshi@njtech.edu.cn (X. Shi), yongwang@njtech.edu.cn (Y. Wang).

https://doi.org/10.1016/j.memsci.2023.122347
Received 30 October 2023; Received in revised form 11 December 2023; Accepted 14 December 2023
Available online 18 December 2023

membranes [23–25]. However, monomers capable of crystallizing into defect-free membranes are limited, posing a challenge to fabricate COF membranes with a wide structural diversity and designability [26]. Moreover, in spite of numerous existing synthetic strategies, there is a scarcity of viable methods to precisely manipulate the pore wall microenvironments of COF membranes [27].

Ionic COFs with evenly distributed charges in their well-defined channels are attractive for the design of pore wall microenvironments [28,29]. Their charge-intensive channels could interact with targeted species to deliver charge-selective separations [30,31]. Nevertheless, the intensive charge repulsion within frameworks in turn impedes the direct crystallization of ionic COFs to form intact and mechanically stable membranes [32]. As a result, the synthetic method of ionic COF membranes remains limited, mostly relying on the pressure-driven stack of delaminated nanosheets [33]. Thus, a novel protocol for the efficient synthesis and amelioration of ionic COF membranes is desired.

Ion-pairing, known as the electrostatic attraction between oppositely charged groups, finds vital applications in organic synthesis and chiral catalysis [34]. The strong Coulomb forces exert a huge impact on reactions involving charged species and intermediates. The design principle of ion-pairing has been demonstrated in the selectivity control of C−H bond functionalization [35]. Given the inborn charges of ionic COFs, we envision an ion-pairing designed protocol to promote the synthesis of ionic COF membranes with improved performance.

In this work, we have demonstrated an ion-pairing strategy for the simultaneous preparation and upgrading of ionic COF membranes. Oppositely charged molecular additives can neutralize the ionic monomers and the synthetic frameworks through ion-pairing. Such neutralization promotes the growth of robust ionic COF layers on porous substrates with a suggested method of electric-driven interfacial crystallization (EDIC, Fig. S1). The optimum guest additives are tightly encapsulated in the generated frameworks, which elevates the membrane selectivity by shrinking the molecular sieving channels. Significantly, the ion-pairing designed membranes demonstrate the recovery and controlled release of bioactive pharmaceuticals, offering great promise for real-world applications.

2. Experimental section

2.1. Materials

1,3,5-Triformylphloroglucinol (Tp, 97 %) and triaminoguanidinium chloride (TG, 98 %) were purchased from Jilin Yanshen Technology. Mesitylene (98 %), 1,4-dioxane (99 %), acetic acid (99.8 %), *N*,*N*-dimethylformamide (DMF, 98 %), 1,3,6,8-pyrenetetrasulfonic acid tetrasodium salt (Na_4PTS, 97 %), tetraoctyl ammonium bromide ([N(n-oct)$_4$]Br, 98 %), tetrabutyl ammonium bromide ([N(n-but)$_4$]Br, 99 %), and alcian blue 8 GX (AB) were supplied by Aladdin. Evans blue (EB), acid fuchsin (AF), methyl orange (MO), chrome black T (CB-T), Congo red (CR), methyl blue (MB), crystal violet (CV), rhodamine B (RB), and hydrochloric acid (HCl, 37 %) were purchased from Beijing Institute of Chemical Reagent. Ethyl acetate (99 %) and polyethylene glycol 400 (PEG400) were obtained from Shanghai Lingfeng Chemical Reagent. Amoxicillin (99 %), vitamin C (99 %), rifampicin (98 %), tetracycline (98 %), spiramycin (98 %), and potassium bromide (KBr, 99 %) were purchased from Macklin. Polyacrylonitrile (PAN, 85 kDa) and nonwoven fabric were purchased from local suppliers. Tetrahydrofuran (THF, 99.5 %), tris(2,2′-bipyridine)ruthenium(II) chloride hexahydrate ($Ru(bpy)_3Cl_2$, 98 %), and sodium sulphate (Na_2SO_4, 98 %) were supplied by Energy Chemicals. Indium-doped tin oxide (ITO) conductive glasses were obtained from Hefei Kejing Material Technology. Deionized water (conductivity: ~2–10 μS cm^{-1}) and ethanol (99.7 %) were used in all the tests. All the reagents and chemicals were used without further purification.

2.2. Solvothermal synthesis of TpTG

Tp (0.2 mmol, 42 mg) and TG (0.2 mmol, 28 mg) were charged into a Pyrex tube (10 × 8 mm^2 and length 18 cm), followed by adding 2 mL of 1,4-dioxane and 0.6 mL of water. The mixture was sonicated for 20 min to achieve sufficient dispersion, after which a degassing process was carried out in liquid N_2 by freeze-pump-thaw procedures for 3 cycles. The tube was then flame sealed and kept at 120 °C for 3 days. The generated TpTG powders were collected by filtration, washed with THF by Soxhlet extraction, and then dried at 80 °C overnight.

2.3. Adsorption tests of TpTG

Aqueous solutions of various charged molecules (25 ppm) were prepared, and 25 mg of TpTG powders were added to 40 mL of the above solutions. The adsorption tests were performed for 48 h at room temperature. The capture ratio was determined by the concentration of charged molecules in the solution using an UV–vis spectrophotometer (NanoDrop 2000C, Thermo Fisher). After adsorption, the TpTG powders were collected by filtration, washed with water and ethanol, and then dried at 80 °C overnight. The resultant powders were denoted as TpTG-*X*, in which *X* stands for the adsorbed molecules. The adsorption stability of the TpTG-*X* powders was also examined. 20 mg of the TpTG-*X* powders were added to 40 mL of water, followed by ultrasonication at 600 W for 2 h. The retention rate of charged molecules was quantified by UV–vis spectroscopy.

2.4. Preparation of PAN substrates

PAN substrates were prepared by non-solvent induced phase separation. PAN powders were dried under vacuum at 80 °C overnight and then dissolved in the mixture of DMF (solvent) and PEG400 (porogen) to form a polymer dope. The mass fractions of PAN, PEG400, and DMF were 11 wt%, 4 wt% and 85 wt%, respectively. The dope was heated under 60 °C for 3 h, stirred at 80 °C for 8 h, and then kept undisturbed for degassing at room temperature overnight to obtain a homogeneous casting solution. To prepare PAN substrates, the above solution was cast on the non-woven fabric using a casting knife with a gate height of 200 μm, which was then immediately immersed into water for phase inversion. Thus-prepared PAN substrates were thoroughly washed and stored in water before further use.

2.5. Ion-pairing designed synthesis of TpTG membranes

Tp (0.43 mmol, 90.3 mg) was dissolved in a mixture of ethyl acetate (36 mL) and mesitylene (174 mL) to form the organic phase. For aqueous phase, TG (0.58 mmol, 81.5 mg) was dissolved in acetic acid aqueous solution (210 mL, 3 mol L^{-1}), followed by the addition of charged additives to reach designated concentrations. The PAN substrate was tightly clamped in the middle of a homemade diffusion cell, and then 70 mL of the two monomer solutions were gently poured into each side of the cell. It should be noted that the top layer of the PAN substrate faced the organic phase. Afterwards, two pieces of ITO conductive glass (length 5 cm × width 2.5 cm) were vertically inserted into both phases with a horizontal distance of 8 cm, and the conductive sides faced each other. The ITO glasses in organic phase and aqueous phase served as the cathode and the anode, respectively. A direct current voltage of 100 V was applied between the two electrodes for membrane synthesis. After designated synthesis durations, the resulting membranes were stored in water after being rinsed with ethanol and water. Thus-prepared membranes were denoted as TpTG@*YZ*, in which *Y* stands for the concentration (ppm) of charged additive *Z* in the aqueous phase. For example, membranes prepared with 20 ppm EB in the aqueous phase were denoted as TpTG@20EB. The neat TpTG membrane free of charged additives was also prepared as a control.

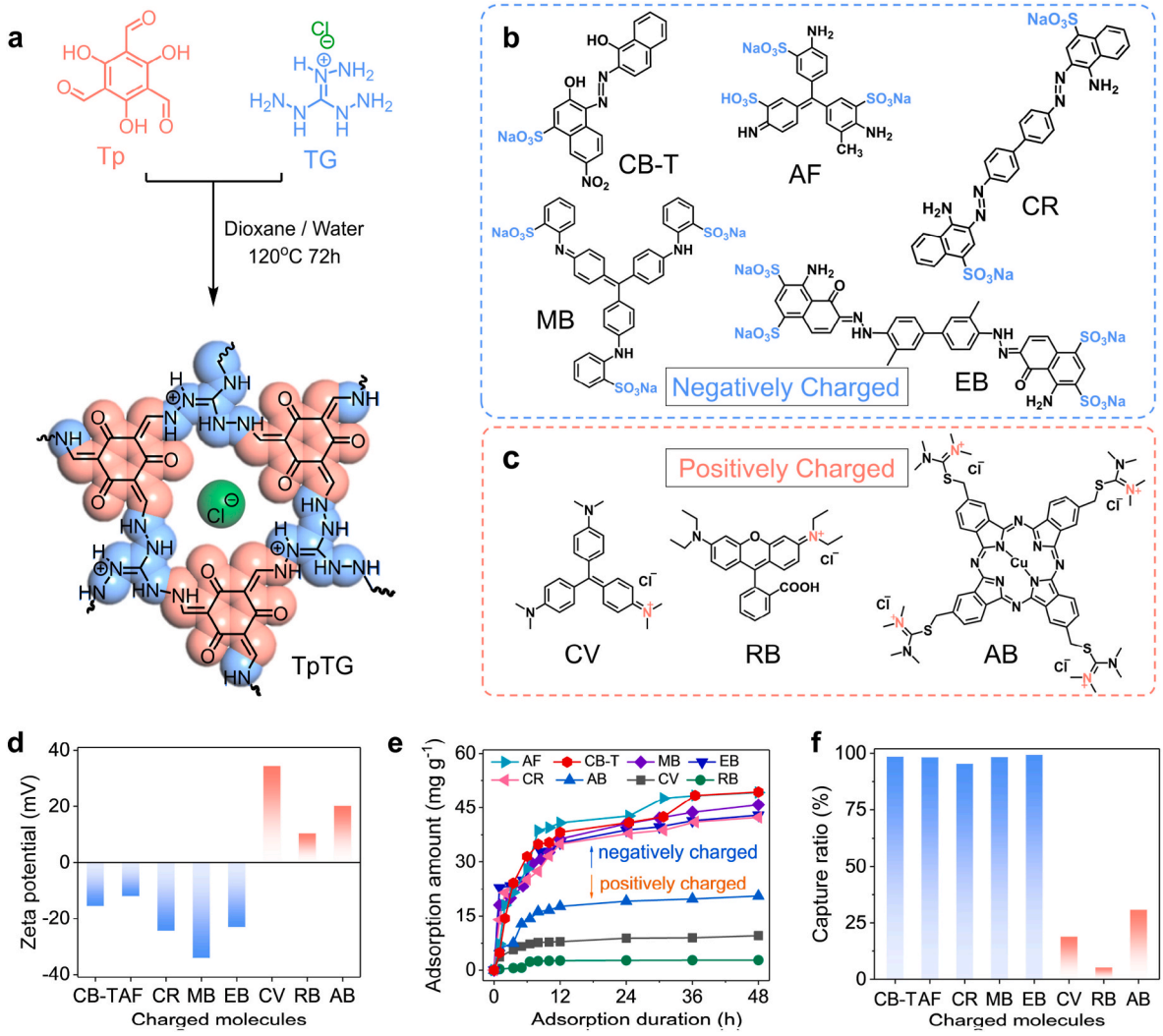

Fig. 1. Adsorption of charged molecules by TpTG powders. (a) Scheme for the synthesis of TpTG. (b, c) Molecular structures of the charged molecules. (d) Zeta potential of the charged molecules. (e) Static adsorption curves of various molecules. (f) Capture ratio of various molecules after 48 h.

2.6. HCl-digesting of the molecule-encapsulated membranes

To determine the actual loading of molecules encapsulated in the membranes, the molecule-encapsulated membranes were digested by immersing in 1 mol L^{-1} HCl aqueous solution for 48 h. The amount of the charged molecules encapsulated in the membranes was calculated according to the absorbance of the digested solutions and the standard curve of molecule solutions using an UV–vis spectrophotometer. The loading of charged molecules was defined as the mass of charged molecules in per unit mass of the molecule-encapsulated membrane (mg g^{-1}).

2.7. Characterizations

A field-emission scanning electron microscope (SEM, Hitachi S-4800) was employed to study the morphologies of the TpTG powders and membranes at an accelerating voltage of 3 kV after Au coating. For transmission electron microscopy (TEM) characterization of the membrane cross-section, the membrane was embedded into epoxy resin and then cut into an 80 nm thick slice using a Leica EM UC7 ultramicrotome. The slice sample was placed onto a copper grid followed by TEM imaging on a FEI Talos F200X G2 microscope at a voltage of 200 kV. Fluorescence images of the membranes were obtained using a fluorescence microscopy (Leica DFC7000T). Fourier transform infrared (FTIR, Nicolet 8700) spectroscopy was utilized to study the chemical compositions of the monomers, TpTG powders and membranes with the wavenumber ranging from 4000 to 1000 cm^{-1}. The attenuated total reflection (ATR) mode and KBr pressed pellet methods were used for membrane and particulate tests, respectively. Elemental analysis was conducted using X-ray photoelectron spectroscopy (XPS, Thermo Fisher Scientific, K-alpha) and energy dispersive X-ray (EDX) mapping. The powder X-ray diffraction (XRD) patterns were measured at room temperature by a Rigaku Smart Lab X-ray diffractometer with Cu Kα radiation ($\lambda = 0.15418$ nm) at 2θ of 2–40° with a step of 0.02° s^{-1}. Nitrogen adsorption-desorption measurements of the TpTG powders were conducted on a surface area and porosity analyzer (Micrometrics ASAP 2460) at 77 K. Brunauer-Emmett-Teller (BET) surface areas and pore size distributions were obtained from the sorption curves based on the nonlocal density functional theory (NLDFT). The surface topography of the membranes was obtained by atomic force microscopy (AFM, XE-100, Park Systems) imaging. Water contact angles of the membranes were obtained using a contact angle goniometer (DropMeter A100, Maist). Surface Zeta potentials of the membranes were performed on a SurPASS electrokinetic analyzer (Anton Paar GmbH) under the streaming potential method. A 0.1 mM of KCl solution was adopted as the background electrolyte solution. The pH values during the test were adjusted by 0.1 M HCl and NaOH aqueous solutions. Liquid Zeta potentials of the solutions were measured by a Malvern Zetasizer Nano ZS90 system.

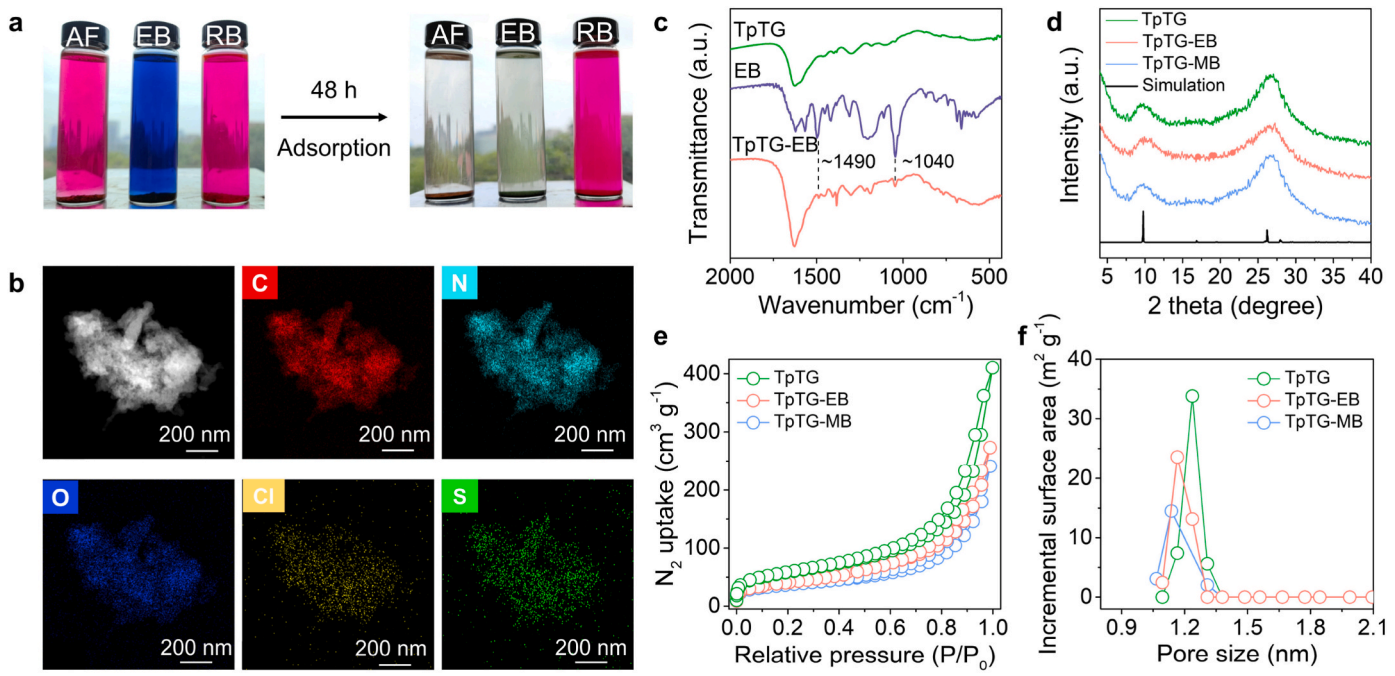

Fig. 2. Characterization of TpTG after molecular adsorption. (a) Photographs of the solutions before and after adsorption. (b) EDX mapping images of TpTG-EB. (c) FTIR spectra of TpTG, EB, and TpTG-EB. (d) XRD patterns, (e) N_2 adsorption-desorption isotherms, and (f) pore size distribution curves of TpTG, TpTG-EB and TpTG-MB.

2.8. Filtration tests

Water permeance and separation performance of the membranes were measured at room temperature under a trans-membrane pressure of 1 bar, using a stirred dead-end filtration cell (Amicon 8003, Millipore). Water permeance (L m^{-2} h^{-1} bar^{-1}) was calculated by the following equation:

$$\text{Water permeance} = V/(AtP)$$

where V (L) stands for the volume of pure water that goes across the effective area A (m^2) of the membrane in a predetermined time t (h) under the trans-membrane pressure P (bar). Separation performance was evaluated using a 25-ppm $Ru(bpy)_3Cl_2$ aqueous solution as the feed. The rejection rate (%) was calculated as:

$$\text{Rejection}=(1-C_p/C_f) \times 100\%$$

where C_p and C_f are the $Ru(bpy)_3Cl_2$ concentrations in the permeate and feed, respectively, which were determined by an UV–vis spectrophotometer. Moreover, for the separation of Na_2SO_4, Na_4PTS, and [N(n-but)$_4$]Br, the concentrations were evaluated by an electrical conductivity meter (S230-K, Mettler-Toledo).

To evaluate the durability of our membrane, a long-term filtration test was performed on the TpEG@20EB membrane using the aforementioned dead-end filtration method. The filtration test lasted for 12 h without interruption, during which the water permeance and Ru $(bpy)_3Cl_2$ rejection were assessed at a 2-h interval.

2.9. Recovery and controlled release of pharmaceuticals

Pharmaceuticals including tetracycline (25 ppm), rifampicin (25 ppm), and spiramycin (10 ppm) were dissolved in water and ethanol as the feeds for drug recovery tests using TpTG@20EB membranes. The rejection rate (%) was calculated as:

$$\text{Rejection}=(1-C_p/C_f) \times 100\%$$

where C_p and C_f are the concentrations of pharmaceuticals in the permeate and feed, respectively, which were determined by an UV–vis spectrophotometer.

For the controlled release experiments, the pharmaceutical-encapsulated membranes were prepared with 40 ppm amoxicillin, vitamin C and rifampicin in the aqueous solutions for 48 h under 100 V. The release experiments were carried out by immersing the above membranes in 25 mL of simulated body fluid (phosphate-buffered saline solution, pH = 7.4) and simulated gastric acid (hydrochloric acid, pH = 2.0) for 6 days. The concentrations of pharmaceuticals in the solutions were measured at specified time intervals using an UV–vis spectrophotometer. The release ratio of pharmaceuticals was calculated according to the standard curves of absorbance and concentration.

3. Results and discussion

3.1. Screening of specific charged additives

Cationic TpTG crystallized from aldehyde Tp and positively charged amine TG was selected as the representative COF for ion-pairing design (Fig. 1a). We studied the structure of TpTG powders produced by solvothermal synthesis. In the FTIR spectra (Fig. S2), the disappearance of –C=O at ~1647 cm^{-1} in Tp and –NH_2 at ~1683 cm^{-1} in TG elucidates the occurrence of Schiff-base reaction between the monomer pairs. The newly formed –C=C at ~1607 cm^{-1} and –C-N at ~1297 cm^{-1} refer to the formation of TpTG with a keto-enamine configuration [36]. EDX mapping images visualize the characteristic elements of C, N, O, and Cl from TpTG (Fig. S3). The XRD measurement depicts obvious diffraction peaks at ~9.7° and ~27° (Fig. S4), which correspond to the (100) and (001) planes, respectively, indicating a crystalline structure [37]. Moreover, N_2 sorption tests manifest the microporous feature (~1.2 nm) of TpTG with a BET surface area of ~204 m^2 g^{-1} (Fig. S5). These spectral and structural determinations confirm the successful synthesis of crystalline TpTG.

To screen eligible charged additives for the ion-pairing design of TpTG, static adsorption of various molecules with designated charges and lateral sizes by TpTG powders was investigated. Fig. 1b–d show the molecular structures and Zeta potentials of these probe adsorbates.

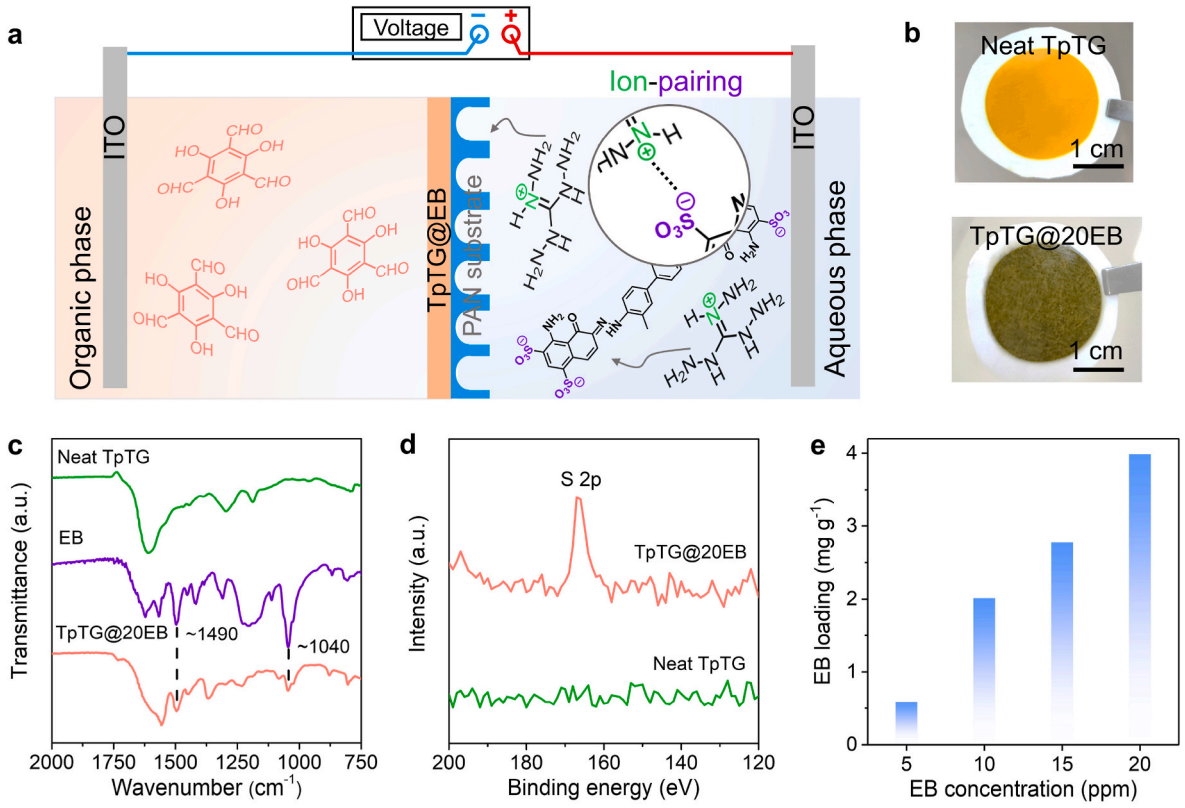

Fig. 3. Ion-pairing designed synthesis of TpTG@EB membranes. (a) Schematic illustration of the ion-pairing designed synthesis. (b) Photographs of the neat TpTG and TpTG@20EB membranes. (c, d) FTIR and XPS spectra of the membranes. (e) EB loadings in the TpTG@EB membranes.

Compared to the positively charged molecules, cationic TpTG exhibits a distinguished affinity to the electronegative ones in terms of both adsorption ratios and rates (Fig. 1e). This distinctive adsorption capability enables effective separation of molecular pairs with opposite charges from their mixture (Fig. S6). Detailed calculations based on the adsorption results give the specific capture ratios toward various molecules (Fig. 1f). TpTG exhibits a rapid and efficient capture (>95 %) of negatively charged molecules irrespective of their lateral sizes, suggesting the dominant role of ion-pairing between cationic TpTG and anionic molecules. Among these electronegative molecules, the capture ratios of EB and MB reach 99.7 % and 98.5 %, respectively, promising for the ion-pairing designed synthesis of TpTG membranes. Moreover, despite the universal adsorption of electronegative molecules, the stability of adsorption relies on their sizes. No leakage of large-sized EB is observed after vigorous ultrasonication treatments, while a slight leakage occurs for small-sized AF (Fig. S7). These findings unravel the importance of charge property and lateral dimension of charged molecules on ion-pairing design [38].

Capture of electronegative molecules as the guest species into microporous TpTG host is revealed by the color contrast of the powders and aqueous solutions (Fig. 2a and Fig. S8). In particular, the aqueous solutions of AF and EB become colorless after adsorption, and the resultant TpTG powders appear the same colors as the captured molecules. By comparison, the RB solution and TpTG-RB remain their initial colors, indicating negligible adsorption due to the inexistence of ion-pairing. With the capture of EB, EDX mapping measurements detect uniformly distributed S element in the TpTG-EB powder (Fig. 2b). We can further observe new peaks agreeing with the guest EB in the FTIR spectra (Fig. 2c). The host-guest interaction causes no damage to the crystallinity of TpTG, as confirmed by the consistent XRD patterns (Fig. 2d). However, the import of additives in the TpTG cavity affects the pore microenvironments [39]. N_2 sorption results verify that the BET surface areas of TpTG powders slightly decrease after adsorbing EB and MB (Fig. 2e). Accordingly, the intake of these large-sized molecules narrows the pore size (Fig. 2f), in line with the molecular shielding effect. The low mass (<1 mg) of the absorbed molecules should be responsible for the observed slight reduction in the pore size of TpTG. Thus, we have identified the validity of ion-pairing design to finely regulate the pore microenvironments of TpTG.

3.2. *Ion-pairing designed synthesis of TpTG membranes*

We sought to explore the feasibility of improving TpTG membranes through ion-pairing design between ionic monomers and charged molecular additives. The ion-pairing designed synthesis of TpTG membranes through EDIC was exemplified using negatively charged EB, as illustrated in Fig. 3a. In this method, both the electronegative EB molecules and the electropositive monomer TG were dissolved in the aqueous solution, and the growth of TpTG membranes will take place at the aqueous-organic interface, which is impervious to the utilization of the organic phase. We should note that the steric effect of guest molecules is expected to be minimal because their dimensions are comparable to the intrinsic pore size of TpTG. To highlight the assistance of electric field on growing ionic COF membranes, specific synthesis conditions are employed, under which the interfacial synthesis without electric field only produces discontinuous TpTG membranes that exhibit no selectivity (Fig. S9a). As a control, the EDIC strategy without adding charged additives allows the growth of TpTG membranes with largely reduced defects under the same conditions (Fig. S9b). This manifests the vital role of the applied electric field, which directs the migration of charged TG to the organic-aqueous interface for efficient crystallization [40]. The effective encapsulation of EB can be visualized by the deepened color of the resultant membranes with the increase of EB concentrations (Fig. 3b and Fig. S10). The FTIR spectra in Fig. 3c show characteristic stretching bands from –C=C and –C-N, revealing that the keto-enol tautomerism remains with the introduction of EB. Fig. 3c also

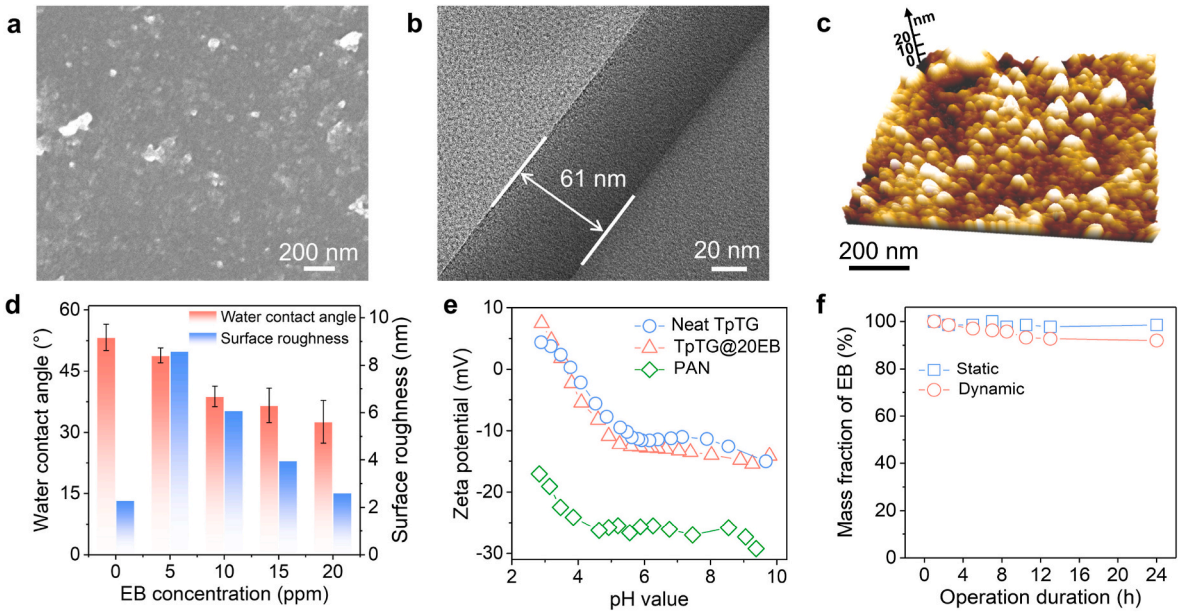

Fig. 4. Membrane characterizations. (a) Surface SEM, (b) cross-sectional TEM, and (c) AFM images of the TpTG@20EB membrane. (d, e) Water contact angle, surface roughness and Zeta potential of the membranes. (f) Ion-pairing stability of the TpEG@20EB membrane.

provides clear evidence that EB is encapsulated into the crystallized TpTG layers, with the presence of characteristic peaks exclusively belonging to EB. The typical element of S detected by XPS and the fluorescence signals further confirm the encapsulation of EB in the TpTG@20EB membrane (Fig. 3d and Fig. S11) [41]. The XRD pattern of the TpTG@20EB membrane with a diffraction peak corresponding to the (100) crystal plane reveals retained crystallinity in spite of the encapsulation of EB molecules (Fig. S12). Of note, the ion-pairing design of TpTG membranes depends on the usage of electric fields. The absence of electric fields leads to no encapsulation of EB (Fig. S13). We quantified the actual EB loadings in the TpTG@EB membranes by digesting in 1 mol L^{-1} HCl, which recognizes the amounts in the range of 0.6–4 mg g^{-1} (Fig. 3e and Fig. S14).

Theoretically, electronegative EB should migrate to the anode instead of the organic-aqueous interface. Indeed, PAN substrates are barely dyed when EDIC is performed without ion-paired TG (Fig. S15). However, as confirmed by Zeta potential results, cationic TG and anionic EB can form combinations in the aqueous solution to neutralize the overall charges (Fig. S16). In the case of EDIC, this ion-pairing neutralization offsets the electric field resistance, thus allowing the movement of oppositely charged EB toward the interface [38]. Considering the overwhelming amount and smaller size of TG compared to EB, the directional migration of TG-EB combinations facilitates the encapsulation of EB in the resultant TpTG membranes. Such encapsulation alleviates the electrostatic repulsion within the frameworks of TpTG and thereby promotes the growth of compact membranes.

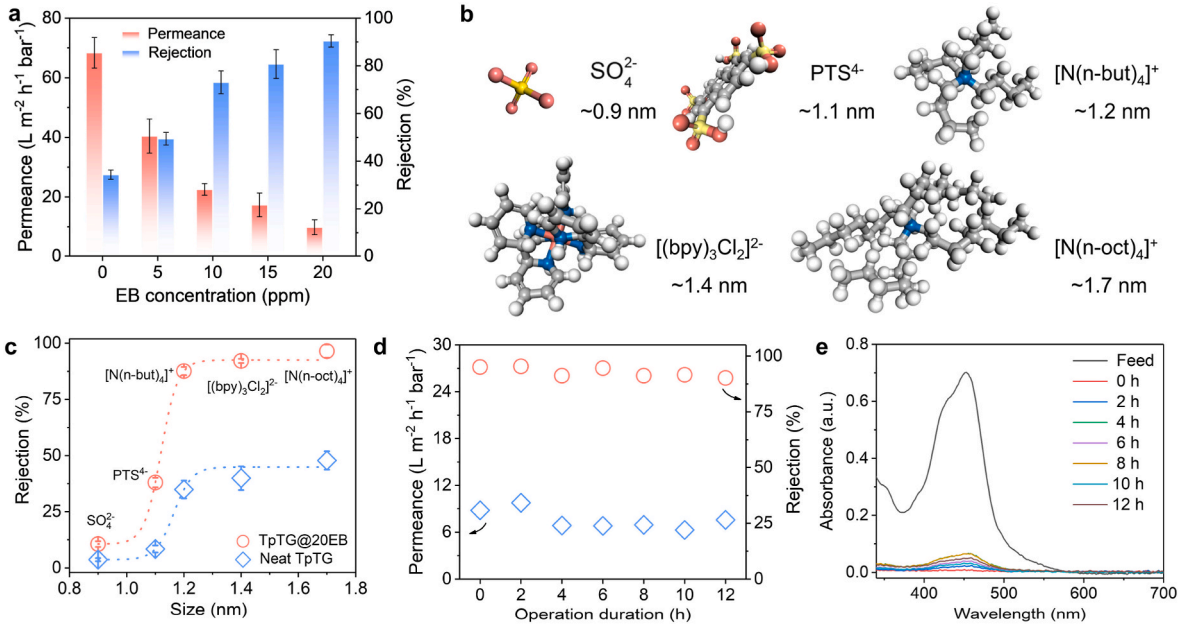

Fig. 5. Evaluation of membrane performance. (a) Pure water permeance and $Ru(bpy)_3Cl_2$ rejection of the TpTG@EB membranes. (b) Molecular structures and sizes of the ionic probes. (c) Rejection profiles of the neat TpTG and TpTG@20EB membranes. (d) Performance stability of the TpTG@20EB membrane. (e) UV–vis spectra in the continuous separation of $Ru(bpy)_3Cl_2$.

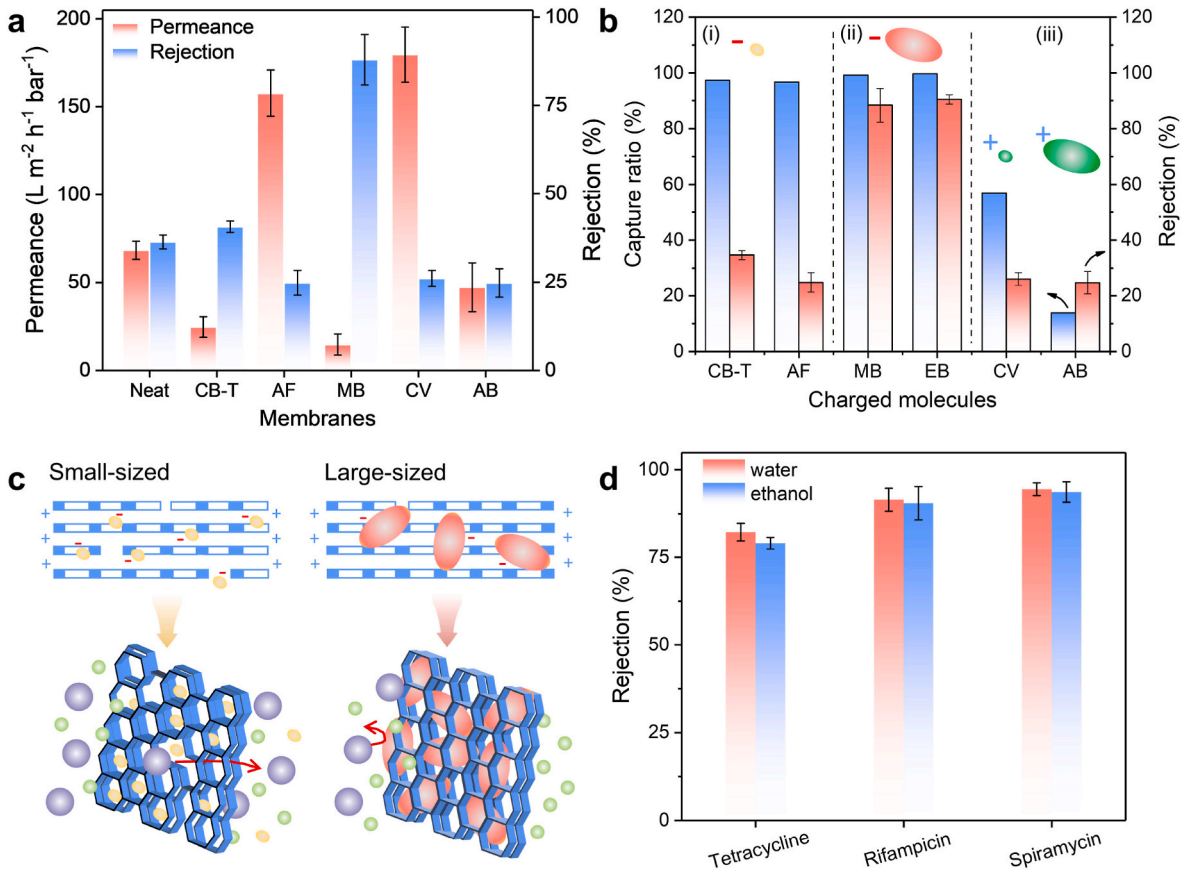

Fig. 6. Study on the separation mechanism of the ion-pairing designed TpTG membranes. (a) Performance of various molecule-encapsulated membranes. (b) Rejection to $Ru(bpy)_3Cl_2$ by the molecule-encapsulated membranes and the corresponding capture ratio. (c) Schematic illustration of the separation mechanism. (d) Rejection to pharmaceuticals by the TpTG@20EB membrane.

We probed into the time-dependent growth of TpTG@EB membranes. As confirmed by SEM imaging, a synthesis duration of 48 h is required to generate dense and defect-free membranes (Fig. S17). Next, we investigated the TpTG@EB membranes synthesized from different EB concentrations with a duration of 48 h. Clearly, well-grown TpTG@EB membranes can be harvested by ion-pairing design with various concentrations of EB (Fig. 4a and Fig. S18), highlighting the validity of our strategy. Cross-sectional SEM images reveal thin and thickness-adjustable TpTG layers on the top of the PAN substrate (Fig. S19). The cross-sectional TEM image in Fig. 4b shows that the TpTG@20EB layer has a uniform thickness of ~61 nm. The increased thickness mostly originates from the ion-pairing of EB, which not only promotes the growth of TpTG but also acts as fillers to thicken the selective layers. AFM examinations show that the resultant TpTG@EB membranes exhibit smooth surfaces with an arithmetic average roughness below 10 nm (Fig. 4c–d and Fig. S20). We can also notice that the membranes display an initial increase followed by a gradual decrease in surface roughness with an increase in EB concentration. This initial rise in roughness could be attributed to the heterogeneous stretching effect of EB fillers, which may become homogeneous to produce smooth membrane surfaces as the amount of the encapsulated EB rises. In addition, the introduction of water affinitive EB improves membrane hydrophilicity [42], which can be confirmed by the reduced water contact angles (Fig. 4d). The Zeta potential curves in Fig. 4e show that the surface electronegativity of the PAN substrate is largely neutralized by the growth of cationic TpTG. Further, compared with the neat TpTG membrane, a slight decrease in Zeta potential of the TpTG@20EB membrane agrees with the encapsulation of electronegative EB [43]. The stability of ion-pairing between EB and TpTG was assessed to demonstrate the operational practicality. As depicted in Fig. 4f, both static and dynamic tests demonstrate stable encapsulation of EB due to the proper match of the charge and molecular size with ionic TpTG.

3.3. Performance evaluation of TpTG@EB membranes

NF performances of the TpTG@EB membranes produced from various EB concentrations were evaluated through water permeance and separation of $Ru(bpy)_3Cl_2$. As shown in Fig. 5a, the neat TpTG membrane free of EB exhibits a water permeance of ~68.4 L m^{-2} h^{-1} bar^{-1} and a low $Ru(bpy)_3Cl_2$ rejection of ~34.4 %. The rejection of $Ru(bpy)_3Cl_2$ increases with the promotion of EB concentrations, ultimately reaching 90.5 % for the TpTG@20EB membrane. Meanwhile, we notice a gradual decline in water permeance to 9.8 L m^{-2} h^{-1} bar^{-1}, which is possibly caused by the rise of membrane thicknesses and the contraction of effective pore sizes [44]. The variation tendency of water permeance and rejection illustrates the potency of ion-pairing on membrane performance. A series of organic and inorganic salts with sizes ranging from 0.8 to 1.8 nm were used to assess the membrane selectivity (Fig. 5b). Rejection profiles of the neat TpTG and TpTG@20EB membranes in Fig. 5c depict an obvious discrepancy in separation precision. High rejections (>85 %) to ionic probes with sizes above 1.2 nm can be achieved by the TpTG@20EB membrane, whereas the neat membrane presents low rejections of <50 % to all the used probes. To be specific, the rejection rate to $[N(n\text{-but})_4]Br$ and $[N(n\text{-oct})_4]Br$ can be increased from 34.9 % and 47.8 % for the neat membrane to 87.6 % and 96.5 % for the TpTG@20EB membrane, respectively. This improved molecular selectivity verifies the upgrade of TpTG membranes through the ion-pairing designed growth of defect-free TpTG layers with a slightly narrowed pore size. These results further indicate that the neat TpTG membrane holds an effective sieving pore size of above 1.7 nm because

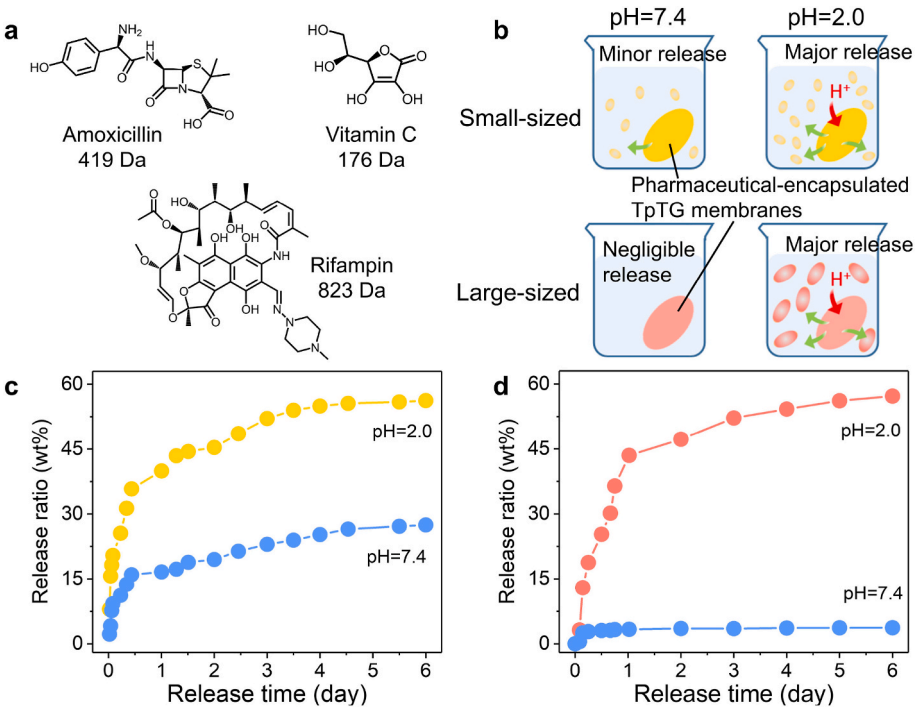

Fig. 7. Controlled release of the bioactive pharmaceuticals by TpTG membranes. (a) Molecular structures of the used pharmaceuticals. (b) Schematic illustration for the controlled release of pharmaceuticals. Release profiles of (c) amoxicillin and (d) rifampin encapsulated in the TpTG membranes.

of the defects, while the ion-pairing designed membrane yields a pore size close to that of the TpTG inherent channel. To reveal the performance stability of the TpTG@20EB membrane, we performed continuous separation tests with a duration of 12 h using 25 ppm $Ru(bpy)_3Cl_2$ aqueous solution as the feed. In this long-term filtration, the membrane selectivity remains basically unchanged, with $Ru(bpy)_3Cl_2$ rejection of 90.2 % after 12 h (Fig. 5d–e), suggesting that the robust ion-pairing promises a lasting operation.

3.4. Separation mechanism of the ion-pairing designed TpTG membranes

We looked deeper into the mechanism of the performance improvements in the ion-pairing designed TpTG membranes. To this end, ion-pairing designed synthesis of TpTG membranes involving other charged additives was carried out (Fig. S21). Most of the resulting membranes receive no promotion in $Ru(bpy)_3Cl_2$ rejection except for the TpTG@20MB membrane (Fig. 6a). We associate this phenomenon with the dimension and charge of guest molecules. As depicted in Fig. 6b, these guest molecules can be classified into three categories, (i) electronegative small-sized molecules, (ii) electronegative large-sized molecules, and (iii) electropositive molecules. Ion-pairing design allows the encapsulation of molecules belonging to the first category, which is proved by the high capture ratios in the adsorption tests; however, these molecules hold small lateral sizes mismatching with the aperture of TpTG. This compromises the ion-pairing efficiency and produces an infirm encapsulation. As a result, the encapsulated molecules spontaneously leak from the TpTG membranes, consistent with the case of TpTG powders (Fig. 6c, **S7** and **S22**), leading to no increase in selectivity. For the third category, the identical charge between guest molecules and TG invalidates the design of ion-pairing regardless of the sizes of these positively charged molecules, yielding no promotion on membranes. In contrast, the utilization of electronegative and large-sized EB and MB promises tight encapsulation of the guest molecules through ion-pairing design of the membranes. And therefore, the resultant TpTG@20MB membrane exhibits a prominent $Ru(bpy)_3Cl_2$ rejection of 88 %. In general, large dimensions and opposite charges are the criteria for the ion-pairing design of ionic COF membranes (Fig. 6c), agreeing with the previous findings on the TpTG powders.

Electrostatic interactions play a dominant role in aqueous NF, which will be weakened in organic solvents [45]. To study the impact of electrostatic interactions on membrane performance, the separation of pharmaceuticals dissolved in water and ethanol was investigated. As demonstrated in Fig. 6d and **S23**, no obvious decline in the rejection rates of the above pharmaceuticals is observed in ethanol compared to those in water. This well-maintained molecular selectivity in ethanol reveals that charge-dependent repulsion is not the main reason for membrane upgrading here [46,47], which should originate from the compact membrane structure with reduced sieving channels [48]. In addition, the high rejection rates (>90 %) of rifampicin and spiramycin in both solvents reveal the potential application of our membrane for pharmaceutical manufacturing [49].

3.5. Controlled release of bioactive pharmaceuticals

Controlled release and delivery of bioactive pharmaceuticals is of vital importance in practical medical treatment [50]. Thanks to their pure organic architecture without toxicity, COFs exhibit favorable biocompatibility that has aroused significant interest in the field of biomedical sciences [51]. In this work, apart from improving the molecular separation performance of membranes, the ion-pairing design also can permit the controlled release of charged additives encapsulated in TpTG membranes. The encapsulated additives can be released depending on the environmental pH values, as well as their charges and sizes. Detailed time-dependent release of the encapsulated charged additives under neutral and acidic conditions was investigated. Figs. S24–S25 show that, different from AF and CV, the release of EB from the TpTG@20EB membrane in an acidic condition is 8-fold faster than that in the neutral case. This pH-responsive release of molecules is promising for controlled delivery of drugs for biological tissues [52]. As a proof-of-concept, negatively charged pharmaceuticals including amoxicillin, vitamin C and rifampin were encapsulated in the TpTG membrane through ion-pairing design (Fig. 7a and **S26-S27**). The

controlled release tests were conducted in simulated body fluid (phosphate-buffered saline solution, pH = 7.4) and simulated gastric acid (hydrochloric acid, pH = 2.0) (Fig. 7b) [53]. We can observe spontaneous releases of small-sized amoxicillin and vitamin C in the simulated body fluid, and the delivery rate effectively increases in the simulated gastric acid (Fig. 7c and **S28-S29**). As a relatively large pharmaceutical, rifampin is released in the simulated gastric acid with a release ratio of 43.5 % after 1 day, which is about 12-fold higher than that in the simulated body fluid (3.6 %) (Fig. 7d). Thus, the demonstration of pH-responsive release enabled by our ion-pairing designed TpTG membranes unravels their practical applicability for controlled and targeted drug delivery in medical treatments.

4. Conclusions

In summary, we have demonstrated an ion-pairing strategy for concurrently crystallizing and improving membranes composed of inherently charged COFs. The lateral dimension and charge nature of guest molecules are demonstrated to be decisive for ion-pairing. The capture of guest molecules in TpTG ultimately reduces the effective pore size without damaging its crystallinity. The application of this ion-pairing strategy in membrane synthesis effectively neutralizes the charges of the ionic monomers and the resultant ionic frameworks. As a result, compact growth of TpTG can be achieved together with the tight encapsulation of the optimum guest molecules within frameworks. The synthesized membranes, featuring narrowed sieving channels, achieve an enhanced rejection of >85 % for organic ions larger than 1.2 nm with a water permeance of ~10 L m^{-2} h^{-1} bar^{-1}. In addition, the membrane performance can be sustained without degradation in continuous operation for 12 h. More importantly, the recovery and controlled release of medically valuable pharmaceuticals are also demonstrated by our membranes. This work provides a novel concept of ion-pairing design to finely engineer COF membranes for multiple practical applications.

CRediT authorship contribution statement

Xingyuan Wang: Data curation, Investigation, Writing – original draft. **Xiansong Shi:** Funding acquisition, Writing – review & editing. **Zhe Zhang:** Investigation. **Congcong Yin:** Investigation. **Zhipeng Zhang:** Investigation. **Yong Wang:** Conceptualization, Funding acquisition, Supervision, Writing – review & editing.

Declaration of competing interest

The authors declare that they have no known competing financial interests or personal relationships that could have appeared to influence the work reported in this paper.

Data availability

Data will be made available on request.

Acknowledgements

This work was supported by the National Natural Science Foundation of China (21825803, 22008110).

Appendix A. Supplementary data

Supplementary data to this article can be found online at https://doi.org/10.1016/j.memsci.2023.122347.

References

[1] A.W. Mohammad, Y.H. Teow, W.L. Ang, Y.T. Chung, D.L. Oatley-Radcliffe, N. Hilal, Nanofiltration membranes review: recent advances and future prospects, Desalination 356 (2015) 226–254.
[2] S. Karan, Z.W. Jiang, A.G. Livingston, Sub-10 nm polyamide nanofilms with ultrafast solvent transport for molecular separation, Science 348 (2015) 1347–1351.
[3] Y. Wen, R.B. Dai, X.S. Li, X.R. Zhang, X.Z. Cao, Z.C. Wu, S.H. Lin, C.Y. Tang, Z. W. Wang, Metal-organic framework enables ultraselective polyamide membrane for desalination and water reuse, Sci. Adv. 8 (2022), eabm4149.
[4] A. He, Z.W. Jiang, Y. Wu, H. Hussain, J. Rawle, M.E. Briggs, M.A. Little, A. G. Livingston, A.I. Cooper, A smart and responsive crystalline porous organic cage membrane with switchable pore apertures for graded molecular sieving, Nat. Mater. 21 (2022) 463–470.
[5] C.C. Yin, Z. Zhang, Z.S. Si, X.S. Shi, Y. Wang, Smart covalent organic frameworks with intrapore azobenzene groups for light-gated ion transport, Chem. Mater. 34 (2022) 9212–9220.
[6] J.T. Liu, S.F. Wang, T.F. Huang, P. Manchanda, E. Abou-Hamad, S.P. Nunes, Smart covalent organic networks (CONs) with "on-off-on" light-switchable pores for molecular separation, Sci. Adv. 6 (2020), eabb3188.
[7] D. Yan, Z. Wang, Z. Zhang, Stimuli-responsive crystalline smart materials: from rational design and fabrication to applications, Acc. Chem. Res. 55 (2022) 1047–1058.
[8] H.W. Peng, W.H. Zhang, W.S. Hung, N.X. Wang, J. Sun, K.R. Lee, Q.F. An, C.M. Liu, Q. Zhao, Phosphonium modification leads to ultrapermeable antibacterial polyamide composite membranes with unreduced thickness, Adv. Mater. 32 (2020), 2001383.
[9] M.C. Zhang, K.C. Guan, Y.F. Ji, G.P. Liu, W.Q. Jin, N.P. Xu, Controllable ion transport by surface-charged graphene oxide membrane, Nat. Commun. 10 (2019) 1253.
[10] Z.W. Jiang, R.J. Dong, A.M. Evans, N. Biere, M.A. Ebrahim, S.Y. Li, D. Anselmetti, W.R. Dichtel, A.G. Livingston, Aligned macrocycle pores in ultrathin films for accurate molecular sieving, Nature 609 (2022) 58–64.
[11] Y.Z. Zhang, D. Kim, R.Q. Dong, X.D. Feng, C.O. Osuji, Tunable organic solvent nanofiltration in self-assembled membranes at the sub-1 nm scale, Sci. Adv. 8 (2022), eabm5899.
[12] J. Shen, Y.C. Cai, C.H. Zhang, W. Wei, C.L. Chen, L.M. Liu, K.W. Yang, Y.C. Ma, Y. G. Wang, C.C. Tseng, J.H. Fu, X.L. Dong, J.Q. Li, X.X. Zhang, L.J. Li, J.W. Jiang, I. Pinnau, V. Tung, Y. Han, Fast water transport and molecular sieving through ultrathin ordered conjugated-polymer-framework membranes, Nat. Mater. 21 (2022) 1183–1190.
[13] F. Sheng, B. Wu, X. Li, T. Xu, M.A. Shehzad, X. Wang, L. Ge, H. Wang, T. Xu, Efficient ion sieving in covalent organic framework membranes with sub-2-nanometer channels, Adv. Mater. 33 (2021), e2104404.
[14] Y.Z. Liang, Y.Z. Zhu, C. Liu, K.R. Lee, W.S. Hung, Z.Y. Wang, Y.Y. Li, M. Elimelech, J. Jin, S.H. Lin, Polyamide nanofiltration membrane with highly uniform sub-nanometre pores for sub-1 angstrom precision separation, Nat. Commun. 11 (2020) 2015.
[15] L. Shen, R.H. Cheng, M. Yi, W.S. Hung, S. Japip, L. Tian, X. Zhang, S.D. Jiang, S. Li, Y. Wang, Polyamide-based membranes with structural homogeneity for ultrafast molecular sieving, Nat. Commun. 13 (2022) 500.
[16] K.Y. Geng, T. He, R.Y. Liu, S. Dalapati, K.T. Tan, Z.P. Li, S.S. Tao, Y.F. Gong, Q. H. Jiang, D.L. Jiang, Covalent organic frameworks: fesign, synthesis, and functions, Chem. Rev. 120 (2020) 8814–8933.
[17] S.Y. Ding, W. Wang, Covalent organic frameworks (COFs): from design to applications, Chem. Soc. Rev. 42 (2013) 548–568.
[18] S.L. Zhang, S. Zhao, X.C. Jing, Z.R. Niu, X. Feng, Covalent organic framework-based membranes for liquid separation, Org. Chem. Front. 8 (2021) 3943–3967.
[19] X. Wang, B. Shi, H. Yang, J. Guan, X. Liang, C. Fan, X. You, Y. Wang, Z. Zhang, H. Wu, T. Cheng, R. Zhang, Z. Jiang, Assembling covalent organic framework membranes with superior ion exchange capacity, Nat. Commun. 13 (2022) 1020.
[20] Z. Wang, S. Zhang, Y. Chen, Z. Zhang, S. Ma, Covalent organic frameworks for separation applications, Chem. Soc. Rev. 49 (2020) 708–735.
[21] H. Wang, Y. Zhai, Y. Li, Y. Cao, B. Shi, R. Li, Z. Zhu, H. Jiang, Z. Guo, M. Wang, L. Chen, Y. Liu, K.-G. Zhou, F. Pan, Z. Jiang, Covalent organic framework membranes for efficient separation of monovalent cations, Nat. Commun. 13 (2022) 7123.
[22] D.B. Shinde, G. Sheng, X. Li, M. Ostwal, A.H. Emwas, K.W. Huang, Z.P. Lai, Crystalline 2D covalent organic framework membranes for high-flux organic solvent nanofiltration, J. Am. Chem. Soc. 140 (2018) 14342–14349.
[23] S.S. Yuan, X. Li, J.Y. Zhu, G. Zhang, P. Van Puyvelde, B. Van der Bruggen, Covalent organic frameworks for membrane separation, Chem. Soc. Rev. 48 (2019) 2665–2681.
[24] Y. Kong, X. He, H. Wu, Y. Yang, L. Cao, R. Li, B. Shi, G. He, Y. Liu, Q. Peng, C. Fan, Z. Zhang, Z. Jiang, Tight covalent organic framework membranes for efficient anion transport via molecular precursor engineering, Angew. Chem. Int. Ed. 60 (2021) 17638–17646.
[25] H. Zhang, X. Li, J. Hou, L. Jiang, H. Wang, Angstrom-scale ion channels towards single-ion selectivity, Chem. Soc. Rev. 51 (2022) 2224–2254.
[26] R. Wang, J.X. Guo, J. Xue, H.H. Wang, Covalent organic framework membranes for efficient chemicals separation, Small Struct 2 (2021), 2100061.
[27] D.B. Shinde, L. Cao, A.D. Wonanke, X. Li, S. Kumar, X.W. Liu, M.N. Hedhili, A. H. Emwas, M. Addicoat, K.W. Huang, Z.P. Lai, Pore engineering of ultrathin covalent organic framework membranes for organic solvent nanofiltration and molecular sieving, Chem. Sci. 11 (2020) 5434.

[28] S. Mitra, S. Kandambeth, B.P. Biswal, M.A. Khayum, C.K. Choudhury, M. Mehta, G. Kaur, S. Banerjee, A. Prabhune, S. Verma, S. Roy, U.K. Kharu, R. Banerjee, Self-exfoliated guanidinium-based ionic covalent organic nanosheets (iCONs), J. Am. Chem. Soc. 138 (2016) 2823–2828.
[29] H.P. Ma, B.L. Liu, B. Li, L.M. Zhang, Y.G. Li, H.Q. Tan, H.Y. Zang, G.S. Zhu, Cationic covalent organic frameworks: a simple platform of anionic exchange for porosity tuning and proton conduction, J. Am. Chem. Soc. 138 (2016) 5897–5903.
[30] W.X. Zhang, L.M. Zhang, H.F. Zhao, B. Li, H.P. Ma, A two-dimensional cationic covalent organic framework membrane for selective molecular sieving, J. Mater. Chem. A 6 (2018) 13331–13339.
[31] X.Y. Wang, J.Y. Yang, X.S. Shi, Z. Zhang, C.C. Yin, Y. Wang, Electrosynthesis of ionic covalent organic frameworks for charge-selective separation of molecules, Small 18 (2022), 2107108.
[32] P.H. Zhang, Z.F. Wang, P. Cheng, Y. Chen, Z.J. Zhang, Design and application of ionic covalent organic frameworks, Coord. Chem. Rev. 438 (2021), 213873.
[33] H. Yang, L.X. Yang, H.J. Wang, Z. Xu, Y.M. Zhao, Y. Luo, N. Nasir, Y.M. Song, H. Wu, F.S. Pan, Z.Y. Jiang, Covalent organic framework membranes through a mixed-dimensional assembly for molecular separations, Nat. Commun. 10 (2019) 2101.
[34] T.E. Schirmer, B. Konig, Ion-pairing catalysis in stereoselective, light-induced transformations, J. Am. Chem. Soc. 144 (2022) 19207–19218.
[35] J.E. Gillespie, A. Fanourakis, R.J. Phipps, Strategies that utilize ion pairing interactions to exert selectivity control in the functionalization of C-H bonds, J. Am. Chem. Soc. 144 (2022) 18195–18211.
[36] Z. Zhang, X.S. Shi, R. Wang, A.K. Xiao, Y. Wang, Ultra-permeable polyamide membranes harvested by covalent organic framework nanofiber scaffolds: a two-in-One strategy, Chem. Sci. 10 (2019) 9077–9083.
[37] H.W. Chen, H.Y. Tu, C.J. Hu, Y. Liu, D.R. Dong, Y.F. Sun, Y.F. Dai, S.L. Wang, H. Qian, Z.Y. Lin, L.W. Chen, Cationic covalent organic framework nanosheets for fast Li-ion conduction, J. Am. Chem. Soc. 140 (2018) 896–899.
[38] H. Tanaka, Y. Kobayashi, K. Furukawa, Y. Okayasu, S. Akine, N. Yasuda, H. Maeda, Pi-stacked ion pairs: tightly associated charged porphyrins in ordered arrangement enabling radical-pair formation, J. Am. Chem. Soc. 144 (2022) 21710–21718.
[39] X. Liu, H. Pang, X. Liu, Q. Li, N. Zhang, L. Mao, M. Qiu, B. Hu, H. Yang, X. Wang, Orderly porous covalent organic frameworks-based materials: superior adsorbents for pollutants removal from aqueous solutions, Innovation 2 (2021), 100076.
[40] R.A. Lehane, A. Gamero-Quijano, S. Malijauskaite, A. Holzinger, M. Conroy, F. Laffir, A. Kumar, U. Bangert, K. McGourty, M.D. Scanlon, Electrosynthesis of biocompatible free-standing pedot thin films at a polarized liquid|liquid interface, J. Am. Chem. Soc. 144 (2022) 4853–4862.
[41] S.F. Chen, C.J. Zhu, W.P. Xian, X.Y. Liu, X.L. Liu, Q.H. Zhang, S.Q. Ma, Q. Sun, Imparting ion selectivity to covalent organic framework membranes using de novo assembly for blue energy harvesting, J. Am. Chem. Soc. 143 (2021) 9415–9422.
[42] W. Hirunpinyopas, E. Prestat, S.D. Worrall, S.J. Haigh, R.A.W. Dryfe, M.A. Bissett, Desalination and nanofiltration through functionalized laminar MoS_2 membranes, ACS Nano 11 (2017) 11082–11090.
[43] M.C. Zhang, P.X. Zhao, P.S. Li, Y.F. Ji, G.P. Liu, W.Q. Jin, Designing biomimic two-dimensional ionic transport channels for efficient ion sieving, ACS Nano 15 (2021) 5209–5220.
[44] H.B. Park, J. Kamcev, L.M. Robeson, M. Elimelech, B.D. Freeman, Maximizing the right stuff: the trade-off between membrane permeability and selectivity, Science 356 (2017) 1137.
[45] P. Marchetti, M.F.J. Solomon, G. Szekely, A.G. Livingston, Molecular separation with organic solvent nanofiltration: a critical review, Chem. Rev. 114 (2014) 10735–10806.
[46] R. Wang, Y.S. Zhou, Y. Zhang, J. Xue, J. Caro, H.H. Wang, Ultrathin covalent organic framework membranes prepared by rapid electrophoretic deposition, Adv. Mater. 34 (2022), 2204894.
[47] T.F. Chen, B. Li, W.B. Huang, C.H. Lin, G.S. Li, H. Ren, Y. Wu, S.H. Chen, W. X. Zhang, H.P. Ma, Highly crystalline ionic covalent organic framework membrane for nanofiltration and charge-controlled organic pollutants removal, Sep. Purif. Technol. 256 (2021), 117787.
[48] X. Shi, Z. Zhang, S. Fang, J. Wang, Y. Zhang, Y. Wang, Flexible and robust three-dimensional covalent organic framework membranes for precise separations under extreme conditions, Nano Lett. 21 (2021) 8355–8362.
[49] X.S. Shi, Z.P. Zhang, C.C. Yin, X. Zhang, J.H. Long, Z. Zhang, Y. Wang, Design of three-dimensional covalent organic framework membranes for fast and robust organic solvent nanofiltration, Angew. Chem. Int. Ed. 61 (2022), e2022075.
[50] F.F. Zheng, W.W. Xiong, S.S. Sun, P.H. Zhang, J.J. Zhu, Recent advances in drug release monitoring, Nanophotonics 8 (2019) 391–413.
[51] S. Bhunia, K.A. Deo, A.K. Gaharwar, 2D covalent organic frameworks for biomedical applications, Adv. Funct. Mater. 30 (2020), 2002046.
[52] F. Huang, W.C. Liao, Y.S. Sohn, R. Nechushtai, C.H. Lu, I. Willner, Light-responsive and pH-responsive DNA microcapsules for controlled release of loads, J. Am. Chem. Soc. 138 (2016) 8936–8945.
[53] S. Das, T. Sekine, H. Mabuchi, T. Irie, J. Sakai, Y. Zhao, Q.R. Fang, Y. Negishi, Three-dimensional covalent organic framework with scu-c topology for drug delivery, ACS Appl. Mater. Interfaces 14 (2022) 48045–48051.